

Strain Hardening in Startup Shear of Long-Chain Branched Polymer Solutions

Gengxin Liu (刘庚鑫),¹ Shiwang Cheng,¹ Hyojoon Lee,² Hongwei Ma,^{1,3} Hongde Xu,^{1,4} Taihyun Chang,² Roderic P. Quirk,¹ and Shi-Qing Wang^{1,*}

¹Department of Polymer Science, Maurice Morton Institute of Polymer Science and Engineering, University of Akron, Akron, Ohio 44325-3909, USA

²Department of Chemistry and Division of Advanced Materials Science, Pohang University of Science and Technology (POSTECH), Pohang 790-784, Korea

³School of Chemical Engineering, Liaoning Key Lab of Polymer Science and Engineering, Dalian University of Technology, Dalian 116024, China

⁴Yanshan Branch of Sinopec Beijing Chemical Industry Institute, Beijing 100013, China

(Received 14 May 2013; published 8 August 2013)

We show for the first time that entangled polymeric liquids containing long-chain branching can exhibit strain hardening upon startup shear. As the significant long-chain branching impedes chain disentanglement, Gaussian coils between entanglements can deform to reach the finite extensibility limit where the intrachain retraction force exceeds the value expected from the usual conformational entropy loss evaluated based on Gaussian chain statistics. The phenomenon is expected to lead to further theoretical understanding.

DOI: 10.1103/PhysRevLett.111.068302

PACS numbers: 83.60.Df, 47.20.-k, 47.50.Gj, 83.10.Kn

Entangled polymeric liquids are extremely complex to model at a molecular level when they are subjected to external deformation at rates that match or exceed the molecular relaxation rates. On the other hand, it is fairly straightforward to carry out macroscopic rheological measurements of such viscoelastic fluids in simple shear and uniaxial extension. Considerable progress has been made in the past several decades to explain nonlinear behavior of entangled polymers in terms of molecular deformation [1–3]. For example, the tube model has been developed [4–7] to describe such nonlinear phenomena as stress overshoot upon startup shear and strain softening associated with the relaxation dynamics after step strain. Since particle-tracking velocimetric observations of strain localization such as shear banding during startup [8], and nonquiescent relaxation after step strain [9] in entangled polymers of linear chains, the tube model has further demonstrated its versatility to claim that it captured all the essential physics associated with these and other instabilities [10–12]. More remarkably, a subsequent extension of the tube theory for entangled polymers with long-chain branching, e.g., low-density polyethylene (LDPE) that has multiple, irregularly spaced long branches [13], attempted to explain why there is “strain hardening” [14,15] in startup uniaxial extension but only “strain softening” in response to startup shear [16–20].

Specifically, based on a simplest long-chain branching architecture involving one crossbar linked on each end to a starlike chains with q arms, a tube-based pom-pom model [18,20] explains that the q arms at the branch point provide an entropic barrier of $qk_B T$ to enable stretching of the crossbar in terms of a stretching factor λ up to the limit of $\lambda^* = q$. The retractive stress develops a *quadratic*

dependence on λ because it arises from both the extension of the crossbar and the tension within the backbone [18]. Since the zero-rate limit is a *linear* response where the transient viscosity $\eta_{E0}^+(t)$ grows linearly in time, the quadratic arguments in the pom-pom model produce “strain hardening” in extension but still extreme strain softening in shear due to the coupling of orientation to chain stretching. Since the publication of the pom-pom model, several *pom-pom-like* systems including H-shaped polymers have been studied to compare with the model. Qualitative agreement between experiment and the model has generally been found [15,18,19,21] for both startup shear and extension.

In this Letter, we study a model LCB polystyrene (PS) made with a straightforward synthetic method [22]. As shown in the schematic drawing in Fig. 1, our comblike PS [23] has an extraordinarily high molecular weight so that even its 22% (volume fraction) solution is sufficiently entangled. Small-amplitude oscillatory shear measurements in Fig. 2 revealed its linear viscoelastic

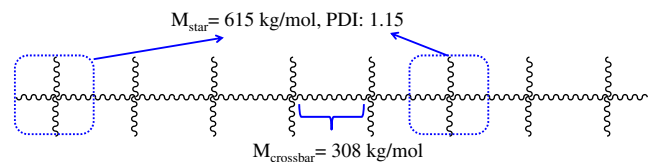


FIG. 1 (color online). (a) Schematic depiction of a relatively monodisperse long-chain branched PS that is made of eight four-arm stars and has total molecular weight of $8 \times 615 = 4920 \text{ kg/mol}$, as determined from temperature gradient interaction chromatography. Each of the seven crossbars has an average molecular weight of 308 kg/mol .

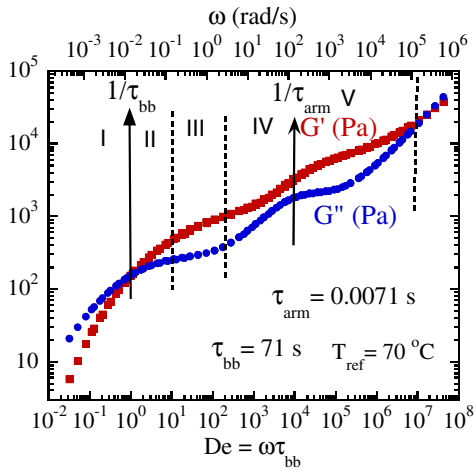


FIG. 2 (color online). Small-amplitude oscillatory shear (SAOS) measurements of the LCB PS solution at a volume fraction of $\phi = 0.22$ and reference temperature $T_{\text{ref}} = 70^\circ\text{C}$. The time-temperature equivalence principle was applied to obtain the linear viscoelastic characterization over nine decades of frequency. The data are presented on double x axes, with the lower given in terms of Deborah number De , and the upper given in terms of the oscillation frequency ω . The lowest frequency portion of storage modulus G' and loss modulus G'' curves are collected at 80°C and the highest frequency portion are obtained with SAOS at -15°C . Other temperatures involved in the SAOS measurements are $70, 25, 0$ and -10°C .

characteristics that resemble the previously reported G' and G'' curves of other melts and solutions made of polymers with LCB [19,21,24,25]. This entangled PS solution is made with a non-volatile solvent, tricresyl phosphate (TCP) from Aldrich 1330-78-5. The glass transition temperature of TCP is -70°C and has a high viscosity of $3\text{ Pa}\cdot\text{s}$ at -15°C . There are two visible plateaus, corresponding to two levels of chain entanglement. This can be anticipated from the depicted chain architecture in Fig. 1, characterized by a modulus $G_0 = \phi^{2.2}G_N^0 \sim 7.15\text{ kPa}$ for $\phi = 0.22$ and $G_N^0 = 0.2\text{ MPa}$ of PS, and $G_{\text{bb}} = (\phi/2)^{2.2}G_N^0 = 1.56\text{ kPa}$, associated with the backbone entanglement.

We impose startup shear to examine nonlinear responses in the various dynamic regimes, using an Anton Paar MCR301 Rheometer equipped with 25 mm cone plate of 2° cone angle (CP25-2-SN4294). As shown in Fig. 3, around the end of the terminal regime ($Wi = \dot{\gamma}\tau_{\text{bb}} < 1$) and for $Wi < 10$ or so, i.e., in regimes I and II, the maximum shear stress occurs at a similar level of strain around 2–3, not much different from the characteristic of linear chains [26,27]. At rates of $\dot{\gamma} = 0.3\text{ s}^{-1}$ and higher (i.e., $Wi = 21 > 10$) in regime III, strong dependence of γ_{max} on $\dot{\gamma}$ shows up. We summarize in Figs. 4(a) and 4(b) the coordinates of the overshoot in comparison to those of linear chains as a function of the applied rate or Wi . The much stronger scaling of $\gamma_{\text{max}} \sim \dot{\gamma}$ in regime III contrasts the scaling behavior of $\gamma_{\text{max}} \sim \dot{\gamma}^{1/3}$ observed in linear

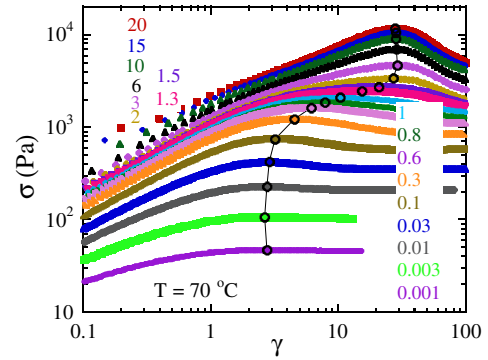


FIG. 3 (color online). Stress-strain curves of startup shear at various rates from 0.001 to 20 s^{-1} at 70°C . Black open cycles marked stress maxima σ_{max} . The coordinates $(\gamma_{\text{max}}, \sigma_{\text{max}})$ of the stress overshoot vary with the applied shear rates differently in the different regimes.

chains [26]. This feature is clearly due to presence of the arms that postpone the onset of catastrophic disintegration of the backbone entanglement network in regime III so that the stress maximum emerges far more gradually than observed in linear chain systems. Another remarkable feature in Fig. 4(a) is a “plateau” in regime IV, where over a range of shear rate γ_{max} reaches a massive value of 30 and remains essentially constant independent of $\dot{\gamma}$.

The data in Figs. 4(a) and 4(b) offer us a first case to compare with the available pom-pom model [18] that derives the stress in terms of a stretching factor λ and orientation function \mathbf{S} as follows

$$\sigma(t) = (15/4)G_{\text{bb}}\phi_b^2\lambda^2(t)\mathbf{S}(t), \quad (1)$$

where the orientation dynamics are given by

$$\frac{\partial}{\partial t}\mathbf{A}(t) = \mathbf{K} \cdot \mathbf{A} + \mathbf{A} \cdot \mathbf{K}^T - \frac{1}{\tau_{\text{bb}}}\left(\mathbf{A} - \frac{1}{3}\mathbf{I}\right), \quad (2)$$

$$\mathbf{S}(t) = \frac{\mathbf{A}(t)}{\text{Tr}[\mathbf{A}(t)]},$$

and the backbone stretching is described by

$$\frac{\partial}{\partial t}\lambda = \lambda(\mathbf{K}:\mathbf{S}) - \frac{1}{\tau_s}(\lambda - 1), \quad \lambda \leq q. \quad (3)$$

A modified pom-pom model [20] introduces drag-strain coupling to rewrite Eq. (3) as

$$\frac{\partial}{\partial x}\lambda = \lambda(\mathbf{K}:\mathbf{S}) - \frac{1}{\tau_s}(\lambda - 1)e^{v^*(\lambda-1)}, \quad v^* = \frac{2}{q-1}. \quad (4)$$

These equations contain two relaxation times: the relaxation time of the backbone, $\tau_{\text{bb}} = (4/\pi^2)\tau_s s_b \phi_b$, and the stretching time, $\tau_s = s_b \tau_{\text{arm}} q$. Here, s_a and s_b are the numbers of entanglement per arm and backbone, respectively, and \mathbf{K} is the deformation rate tensor. The backbone volume fraction ϕ_b is defined as $\phi_b = s_b/(2qs_a + s_b)$.

Equation (2), along with either Eq. (3) or Eq. (4), is solved by MATLAB using the command ODE45, based on the

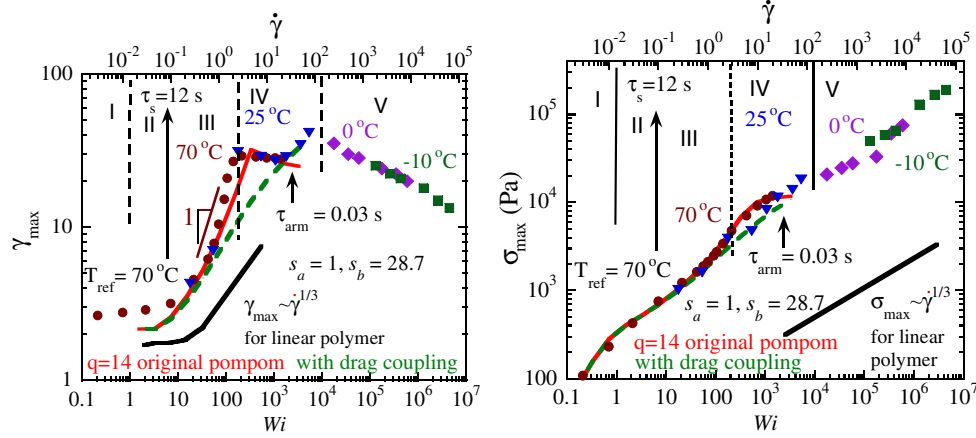


FIG. 4 (color online). (a) The strain, γ_{\max} , at the peak shear stress σ_{\max} , plotted against the imposed shear rates given in double x axes, with the lower one given in terms of the Weissenberg number $Wi = \tau_{bb} \dot{\gamma}$, and the upper one given in terms of the shear rate $\dot{\gamma}$, at the reference temperature of 70°C . The data involve startup shear experiments at four different temperatures of 70 , 25 , 0 , and -10°C . The WLF shifting factor is 25 between 70 and 25°C , 33 between 25 and 0°C and 242 between 25 and -10°C . (b) The peak shear stress σ_{\max} , plotted against the imposed shear rate, given in the same double x axes as defined in (a).

following choices of the parameters: $q = 14$, $s_b = 28.7$, $s_a = 1$, $\tau_{\text{arm}} = 0.03$ s, $G_{bb} = 1560$ Pa, $\tau_{bb} = 71$ s, and $\tau_s = 12$ s, to achieve a good fit. The solutions are inserted into Eq. (1) to produce the solid curves according to Eq. (3) and dashed curves according to Eq. (4) in Figs. 4(a) and 4(b), respectively. The solid curve has a plateau region where γ_{\max} is flat with increasing rate, matching the plateau of the data in Fig. 4(a). On the other hand, the data in Fig. 4(b) do not appear to level off as indicated by the theoretical solid line. The theoretical dashed lines from the updated pom-pom model do not reveal a plateau for either of the two figures. We presented these calculations only up to the rate of $1/\tau_{\text{arm}}$ since the pom-pom model is not developed to describe entanglement of arms and therefore not suitable to predict nonlinear behavior at higher rates. From regime I to IV, the agreement between our data and the pom-pom model is rather promising, given the fact that our LCB is not a simple pom-pom molecule modeled by the theory. For linear chains, disentanglement always occurs in simple shear before the finite extensibility limit is approached. In contrast, entanglements can get locked-in during fast startup uniaxial extension [28] to show true strain hardening [29].

Can LCB delay the disentanglement to the point where the finite extensibility limit is reached even in startup shear? In other words, is shear strain hardening due to non-Gaussian stretching possible in our LCB PS solution? Up to regime IV there is only the sign of strain softening. Moreover, the pom-pom model would only anticipate shear strain softening because of the coupling between chain orientation and stretching. But LCB is expected to play a greater role when the arms are engaged in entanglement. This means application of higher rates in the regime V. By conducting the startup shear experiments at -10°C , Fig. 5 shows a typical set of startup shear at equivalent rates

from 1815 (0.3) to $60\,500$ (10) s^{-1} for $T_{\text{ref}} = 70^\circ\text{C}$. Stress responses at these effectively very high rates are sharply different from the strain softening observed at the lower rates probed at 70°C as shown in the inset. The initial response exhibits an elastic modulus comparable to G_0 , confirming that the primary entanglement network with participation of arms is undergoing elastic deformation. However, this network quickly yields after a few strain units, as expected from the relatively short arms, leaving the backbones to withstand further shearing, at the four lowest rates. The backbone network shows no sign of yielding, however. More remarkably, after a shear strain of ca. 10 – 15 , σ takes an upturn to grow more strongly than linearly with γ . The strain hardening, indicated by the upturn in the stress vs strain plot on linear scales, implies that non-Gaussian stretching has occurred. In other words, the Gaussian coils between entanglements may have been

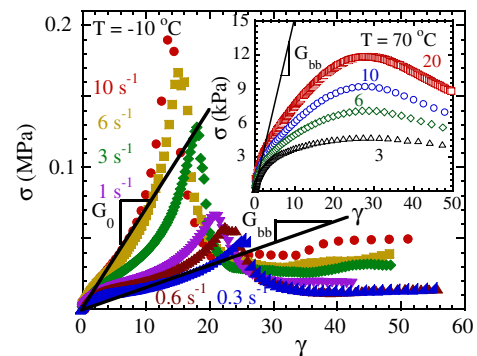


FIG. 5 (color online). Stress vs strain plot shows non-Gaussian stretching and "strain hardening" in startup simple shear at -10°C , starting at 0.3 s^{-1} , which equivalent to 1815 s^{-1} at 70°C . Inset is Fig. 3 replotted on the linear-linear scale to show the usual strain softening.

straightened at such high strains. In the affine deformation limit, the condition to straighten the backbone entanglement strand (BES) can be readily estimated as requiring a strain of $\gamma_{\text{BES}}^* = L_{\text{BES}}/R_{\text{BES}} = (N_e)^{1/2} = (\phi/2)^{-0.6} \lambda_{\text{eq}}^* = 16$, where $N_e = N_{e0}(\phi/2)^{-1.2}$, $\phi = 0.22$, and $\lambda_{\text{eq}}^* = (N_{e0})^{1/2} = 4.3$. Indeed, the upturns in Fig. 5 take place around strains just below γ_{BES}^* .

At the two highest rates, the primary network hardly yields because the shear stress follows closely $\sigma(t) = G_0\gamma(t)$. For $\gamma > 11$, σ deviates upward from the linear relation given by the inclined line, indicating strong non-Gaussian responses. Thus, depending on the value of the imposed shear rate, either the backbone network (G_{bb}) or the primary network (G_0) displays strain hardening, i.e., becoming stiffer with increasing external deformation. This is the first report of shear strain hardening for entangled polymeric liquids and thus has rather significant theoretical implications.

It is evident that the present solution can reach the finite extensibility limit because the LCB prevented chain disentanglement from taking place prematurely. Because of the presence of branch points, more severe molecular straining of the entanglement network can take place before any eventual chain disentanglement. The observed strain hardening of the present system underscores that simple shear can effectively stretch the entanglement network made of LCB regardless of chain orientation. Given the mesh size of the entanglement network, on the order of $a = a_0(\phi/2)^{-0.6} \sim 30$ nm, the molecular tension f within a backbone entanglement strand can be estimated as $f \sim a^2\sigma_{\text{max}} \sim 0.1$ nN, whereas the force required to break the covalent bond is known to be several nN. Thus, the cause for the sharp strain softening beyond the peak stresses in Fig. 5 remains elusive and needs to be explored in a future study.

In summary, the LCB PS solutions show a rich variety of transient responses to startup shear at different rates from regime I to V. At low rates, the arms act like a solvent to swell the backbone entanglement network, and the comb-like molecules behave like linear chains. The nonlinear rheological responses at low rates can be qualitatively described using the tube model although a different interpretation also exists for the origin of the stress overshoot [30]. The most remarkable behavior is the shear strain hardening observed in regime V where the effect of LCB, i.e., the presence of branch points, is remarkable. We conclude that the observed strain hardening is a result of the molecular deformation reaching the finite extensibility limit. The non-Gaussian response is made possible by the presence of LCB that defers chain disentanglement. This first report of strain hardening upon startup shear of entangled polymeric liquids indicates that more theoretical development is needed.

This work is supported, in part, by National Science Foundation Grant No. DMR-1105135.

*Corresponding author.

swang@uakron.edu

- [1] M. Doi and S.F. Edwards, *The Theory of Polymer Dynamics* (Oxford University Press, Oxford, 1986).
- [2] H. Watanabe, *Prog. Polym. Sci.* **24**, 1253 (1999).
- [3] T. C. B. McLeish, *Adv. Phys.* **51**, 1379 (2002).
- [4] G. Ianniruberto and G. Marrucci, *J. Non-Newtonian Fluid Mech.* **65**, 241 (1996); *J. Rheol.* **45**, 1305 (2001).
- [5] D.W. Mead, R. G. Larson, and M. Doi, *Macromolecules* **31**, 7895 (1998).
- [6] S. T. Milner, T. C. B. McLeish, and A. E. Likhtman, *J. Rheol.* **45**, 539 (2001).
- [7] R. G. Graham, A. E. Likhtman, T. C. B. McLeish, and S. T. Milner, *J. Rheol.* **47**, 1171 (2003).
- [8] P. Tapadia and S. Q. Wang, *Phys. Rev. Lett.* **96**, 016001 (2006).
- [9] S. Q. Wang, S. Ravindranath, P. Boukany, M. Olechnowicz, R. Quirk, A. Halasa, and J. Mays, *Phys. Rev. Lett.* **97**, 187801 (2006).
- [10] J. M. Adams and P. D. Olmsted, *Phys. Rev. Lett.* **102**, 067801 (2009); S. Q. Wang, *Phys. Rev. Lett.* **103**, 219802 (2009).
- [11] A. Lyhne, H. K. Rasmussen, and O. Hassager, *Phys. Rev. Lett.* **102**, 138301 (2009).
- [12] J. M. Adams, S. M. Fielding, and P. D. Olmsted, *J. Rheol.* **55**, 1007 (2011).
- [13] E. Nordmeier, U. Lanver, and M. D. Lechner, *Macromolecules* **23**, 1077 (1990).
- [14] J. Meissner, *J. Appl. Polym. Sci.* **16**, 2877 (1972).
- [15] D. J. Read, D. Auhl, C. Das, J. den Doelder, M. Kapnistos, I. Vittorias, and T. C. B. McLeish, *Science* **333**, 1871 (2011).
- [16] D. K. Bick and T. C. B. McLeish, *Phys. Rev. Lett.* **76**, 2587 (1996).
- [17] G. Bishko, T. C. B. McLeish, O. G. Harlen, and R. G. Larson, *Phys. Rev. Lett.* **79**, 2352 (1997).
- [18] T. McLeish and R. Larson, *J. Rheol.* **42**, 81 (1998).
- [19] T. C. B. McLeish *et al.*, *Macromolecules* **32**, 6734 (1999).
- [20] R. J. Blackwell, T. C. B. McLeish, and O. G. Harlen, *J. Rheol.* **44**, 121 (2000).
- [21] J. K. Nielsen, H. K. Rasmussen, M. Denberg, K. Almdal, and O. Hassager, *Macromolecules* **39**, 8844 (2006).
- [22] G. X. Liu, H. Ma, H. Lee, H. Xu, S. Cheng, T. Chang, R. P. Quirk, and S. Q. Wang, *Macromolecules* (to be published).
- [23] H. Lentzakis, D. Vlassopoulos, D. J. Read, H. Lee, T. Chang, P. Driva, and N. Hadjichristidis, *J. Rheol.* **57**, 605 (2013), where real comb polymers were made and studied.
- [24] D. R. Daniels, T. C. B. McLeish, B. J. Crosby, R. N. Young, and C. M. Fernyhough, *Macromolecules* **34**, 7025 (2001).
- [25] M. Kapnistos, D. Vlassopoulos, J. Roovers, and L. G. Leal, *Macromolecules* **38**, 7852 (2005).
- [26] S. Ravindranath and S. Q. Wang, *J. Rheol.* **52**, 681 (2008).
- [27] F. Snijkers and D. Vlassopoulos, *J. Rheol.* **55**, 1167 (2011).
- [28] H. Sun and S. Q. Wang, *Sci. China: Chem.* **55**, 779 (2012).
- [29] G. X. Liu, H. Sun, S. Rangou, K. Ntetsikas, A. Avgeropoulos, and S.-Q. Wang, *J. Rheol.* **57**, 89 (2013).
- [30] S. Q. Wang, Y. Y. Wang, S. W. Cheng, X. Li, X. Y. Zhu, and H. Sun, *Macromolecules* **46**, 3147 (2013).